



**HAL**  
open science

## **Influence of the variability of soil profile properties on weak and strong seismic response**

Stefania Gobbi, Luca Lenti, Maria Paola Santisi D'avila, Jean-François Semblat,  
Philippe Reiffsteck

### ► **To cite this version:**

Stefania Gobbi, Luca Lenti, Maria Paola Santisi D'avila, Jean-François Semblat, Philippe Reiffsteck. Influence of the variability of soil profile properties on weak and strong seismic response. *Soil Dynamics and Earthquake Engineering*, 2020, 135, pp.106200. <10.1016/j.soildyn.2020.106200>. <hal-03238056>

**HAL Id: hal-03238056**

**<https://hal.science/hal-03238056v1>**

Submitted on 26 May 2021

**HAL** is a multi-disciplinary open access archive for the deposit and dissemination of scientific research documents, whether they are published or not. The documents may come from teaching and research institutions in France or abroad, or from public or private research centers.

L'archive ouverte pluridisciplinaire **HAL**, est destinée au dépôt et à la diffusion de documents scientifiques de niveau recherche, publiés ou non, émanant des établissements d'enseignement et de recherche français ou étrangers, des laboratoires publics ou privés.



HAL Authorization

1 **Influence of the variability of soil profile properties on weak and strong seismic response**

2

3 Stefania Gobbi<sup>a,\*</sup>, Luca Lenti<sup>a,d</sup>, Maria Paola Santisi d'Avila<sup>b</sup>, Jean-François Semblat<sup>c</sup>,

4 Philippe Reiffsteck<sup>a</sup>

5

6 <sup>a</sup> Université Gustave Eiffel, IFSTTAR (GERS/SRO), Marne la Vallée, France

7 <sup>b</sup> Polytech'Lab, EA UNS 7498, Université Côte d'Azur, Sophia Antipolis, France

8 <sup>c</sup> IMSIA (UMR9219), CNRS, EDF, CEA, ENSTA Paris, Institut Polytechnique de Paris,

9 France

10 <sup>c</sup> Cerema, Equipe-Projet MOUVGS, Sophia Antipolis, France

11

12

13 Corresponding author:

14 Stefania Gobbi

15 Université Gustave Eiffel, IFSTTAR (GERS/SRO)

16 14-20 Boulevard Newton - 77420 Champs sur Marne - France

17 Email: [stefania.gobbi@ifsttar.fr](mailto:stefania.gobbi@ifsttar.fr)

18

19 **ABSTRACT**

20 Characterizing the potential effect of local site conditions on the amplification of ground  
21 motions is a critical aspect of seismic hazard and risk assessment. The aim of this study is to  
22 investigate the reliability and the limit of using the average shear wave velocity in the upper  
23 30m of the soil profile  $v_{s,30}$ , as single proxy, to characterize seismic site effects for weak and  
24 strong events.

25 To this regard, a dataset of 300 one-dimensional soil profiles with a given  $v_{s,30}$  are generated  
26 through a Monte Carlo approach. Their seismic responses are computed for a set of 40 real  
27 accelerograms, with different seismic features. The vertical propagation from the bottom of  
28 the generated columns is modeled using a finite element spatial discretization, accounting for  
29 both linear and nonlinear soil behavior.

30 The site dominant frequency  $f_0$  and the shear wave velocity gradient in the profile  $B_{30}$  are  
31 proposed as proxies to characterize seismic site effects and the variability of the response  
32 spectra for the numerical signals, at the free surface of the set of columns, is discussed.  
33 Correlations between site-specific amplification factors deduced using the numerical response  
34 spectra and the proposed site proxies are analyzed for different sub-ranges of periods. The  
35 obtained amplification factors are then compared to those proposed by different international  
36 and national design codes.

37 The results, obtained under assumption of linear and nonlinear behavior of soil, emphasize the  
38 need to introduce complementary site parameters proxies, in addition to  $v_{s,30}$ , to characterize  
39 the expected site effects in design response spectra.

40

41 **Keywords:** Geotechnical properties, site effects, variability, average shear wave velocity,  
42 impedance contrast, response spectrum, Eurocode 8.

43

## 44 **1. Introduction**

45 Recent and past earthquakes, such as 1985 Mexico City, 1989 Loma Prieta, 1994  
46 Northridge, 1995 Kobe events, among others, underline the need to characterize the effect  
47 of the local soil conditions on seismic site response prediction. It has been widely recognized  
48 that the seismic site effects are generally related to the stratigraphy, the surface topography,  
49 the impedance contrast and the rheology of the soils involved during the propagation of  
50 seismic waves [1].

51 Current seismic design codes consider the seismic site effects through a ground type  
52 classification solely based on the average shear velocity in the upper 30m of the soil profile  
53  $v_{s,30}$  proposed by Borchardt [2], neglecting the depth of the bedrock and the property of the  
54 soil below 30m. Nevertheless, it has been recognized that  $v_{s,30}$  is a useful parameter to capture  
55 some features of the local site amplification effects [3–7].

56 However, several researches [8–15] show that  $v_{s,30}$  cannot be used as the single-site proxy to  
57 discriminate soils in terms of seismic amplification over the whole frequency range of  
58 interest. To this regard, Steidl [16] and Park and Hashash [8] recommended the introduction  
59 of a depth-to-bedrock parameter since they found that the provisions based on  $v_{s,30}$  are over  
60 and under conservative for deep sediments at short and long periods, respectively. Many  
61 alternatives to  $v_{s,30}$  are proposed to improve site soil characterization accounting for  
62 additional information on the shear wave velocity profile with depth, the site dominant  
63 frequency  $f_0$ , the impedance contrast between sediments and bedrock and the depth to the  
64 bedrock.

65 Various studies [11,12,17–21] propose new site classification based on a combination of these  
66 different proxies. Gallipoli and Mucciarelli [21] and Cadet et al. [11] propose a two-  
67 parameters site classification approach through the dominant frequency  $f_0$  and the average

68 shear wave velocity  $v_s(\bar{z})$  in the shallow soil up to the reference depth  $\bar{z}$ . Kotha et al. [17]  
69 introduce a new approach classification characterized by the kernel density distributions of  
70  $v_{s,30}$ ,  $v_{s,10}$ ,  $H_{800}$  and the predominant period.

71 Recently, several researchers explore the performance of different site proxies in order to  
72 reduce the aleatory variability on the seismic prediction. Derras et al. [14] investigate the  
73 performance of four site condition proxies,  $v_{s,30}$ ,  $f_0$ , the topographical slope and the depth  
74  $H_{800}$  (the depth where the shear wave velocity  $v_s$  reaches 800 m/s) using a neural networks  
75 approach, in order to assess their benefits to reduce the uncertainty of the site response. They  
76 conclude that the best single-proxy is  $v_{s,30}$  for periods below 0.6 s and  $f_0$  or  $H_{800}$  at longer  
77 periods and that the best pair is  $(v_{s,30}, H_{800})$  at short periods and  $(f_0, H_{800})$  at long periods.

78 Stambouli et al. [22] conduct a numerical investigation on 858 soil columns corresponding to  
79 real sites profiles from Japan, USA, and Europe. They show that the best performing site  
80 proxy is the impedance contrast between bedrock velocity and minimum surface velocity but  
81 even the pair  $(v_{s,30}, f_0)$  can reduce significantly the variability of the site response at least  
82 around 60%.

83 Lately, Chuanbin et al. [23] study the best performing site proxies for the linear  
84 characterization of the site response using 1840 ground-motion recordings from a KiK-net  
85 database. They focus their study on the dominant period of the site  $T_0$ , the site depths  $Z_{0.8}$   
86 and  $Z_{1.0}$ , which are measured site depths to layers having shear-wave velocity 0.8 and 1.0  
87 km/s, respectively. They demonstrate that predictions based on the configuration using  $T_0$  as  
88 the primary and  $v_{s,30}$  as the secondary proxy can induce a significant reduction in site-to-site  
89 amplification variability.

90 Ciancimino et al. [24] adopt some classical proxies for site characterization in the context of

91 seismic site effect estimation. Their reliability is evaluated, under the assumption of linear  
92 regime, and compared to the ground type classification adopted in the Eurocode 8 [25], New  
93 Zealand Standard [26] and that suggested by Pitilakis et al. [18].

94 Following these recent reviews, the prediction of the seismic site response using only a single  
95 proxy over the whole period range does not seem satisfactory. Hence, to improve the site  
96 amplification estimation, it is advisable to use a combination of site proxies rather than a  
97 single site proxy. Based on this idea, the goal of the present research is to assess the  
98 correlation with the site amplification of some site parameters used to characterize the site  
99 condition, with the aim of improving the expected ground motion prediction.

100 In this research, the site dominant frequency  $f_0$  and the shear wave velocity gradient  $B_{30}$  are  
101 selected as complementary proxies, in addition to  $v_{s,30}$ , and applied to a wide variety of soil  
102 profiles with given  $v_{s,30}$  and  $H_{800}$ . The two proposed proxies has been selected because they  
103 can be estimated, without excessive cost, by geophysical methods applied to ambient  
104 vibrations or seismic motions, recorded using temporary instruments located at the soil  
105 surface [27].

106 Then, since the nonlinear behavior of soils has been recognized as an important factor in site  
107 response [28,29], the second aim of this work is to explore how these site parameter proxies  
108 allow to capture and account for the nonlinear component of site response.

109

## 110 **2. Methodology**

111 The stratigraphy of a set of soil profiles with a given average shear wave velocity in the upper  
112 30m  $v_{s,30}$  is randomly generated, according to the Monte Carlo method. Consequently, all the  
113 generated profiles belong to the same ground type in the Eurocode classification [25].

114 The seismic wavefield along these soil profiles has been computed using the finite element  
115 method (FEM) for spatial discretization and the Newmark algorithm for time discretization,

116 implemented in the SWAP\_3C FEM package [30,31]. The highest-amplitude horizontal  
117 component of a wide variety of recorded earthquakes, representative of regions of low to  
118 moderate intensity, is applied as input motion at the base of each soil profile. These recorded  
119 signals are propagated along each soil profile and the ground response at the surface is  
120 evaluated in both cases of linear and nonlinear soil behavior.

121 Results are presented with regard to the amplification factors adopted by Ciancimino et al.  
122 [24], in different period ranges, in order to distinguish short-, mid- and long-period  
123 amplification factors. Differences between the response spectra of numerical signals at the  
124 soil surface and the reference spectrum proposed by European buildings codes [25] are then  
125 quantified and discussed.

126

## 127 **2.1 Set of generated soil profiles for the statistical analysis**

128 The parameters chosen for the set of soil profiles are the average shear wave velocity  
129  $v_{s,30} = 270 \text{ m/s}$ , corresponding to the ground type C according to the Eurocode 8 [25], the soil  
130 depth of 30m, the number of layers equal to 4 and the density  $\rho = 1850 \text{ kg/m}^3$ . The  
131 geotechnical properties assumed for the bedrock are the density  $\rho_b = 2200 \text{ kg/m}^3$  and the  
132 shear wave velocity  $v_{sb} = 1000 \text{ m/s}$ .

133 The properties of each layer are generated considering each stochastic parameter uniformly  
134 distributed in a given range. The soil layer thickness ranges in  $[1-15 \text{ m}]$ , the shear wave  
135 velocity in  $[100-800 \text{ m/s}]$  and 4 soil types can be randomly targeted.

136 Each soil type from 1 to 4 is associated to a plasticity index  $PI = 0,5,10$  and  $20\%$ ,  
137 respectively. Yokota et al. [32] have shown that normalized shear modulus reduction curve  
138 for different types of soils can be expressed by a set of formulas in the absence of available  
139 test data. To this regard, a normalized shear modulus reduction curve, as a function of the

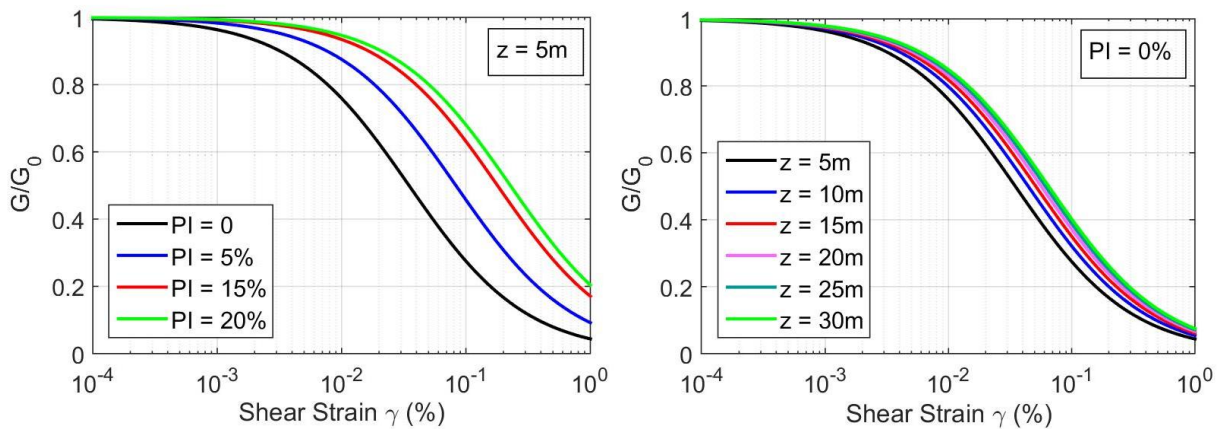
140 shear strain  $\gamma$ , is derived using the four-parameter model proposed by Darendeli [33] to  
 141 characterize normalized modulus reduction formulation:

$$142 \quad G(\gamma)/G_0 = 1 / \left[ 1 + (\gamma/\gamma_r)^\alpha \right] \quad (1)$$

143 assuming a normal consolidated soil (over-consolidation ratio  $OCR=1$ ). The reference shear  
 144 strain is defined as  $\gamma_r = (\phi_1 + \phi_2 PI \cdot OCR^{\phi_3}) \sigma'_{v0}{}^{\phi_4}$ , where from  $\phi_1$  to  $\phi_4$  are parameters that  
 145 relate the normalized modulus reduction curve to soil type and loading conditions estimated  
 146 on the basis of statistical analysis ( $\phi_1 = 0.0352$ ,  $\phi_2 = 0.001$ ,  $\phi_3 = 0.3246$ ,  $\phi_4 = 0.3483$ ) and  
 147  $\alpha = 0.92$ .

148 The vertical effective stress  $\sigma'_{v0}$  is calculated each 5m using the chosen soil density  
 149  $\rho = 1850 \text{ kg/m}^3$ , to account for the variation of the shear modulus decay curve with depth.

150 The normalized shear modulus reduction curves employed for the four soil types, associated  
 151 to a different plasticity index  $PI$  are shown in Fig. 1 (a), for a fixed depth  $z = 5 \text{ m}$ . The curves  
 152  $G(\gamma)/G_0$  at various depths, associated to a related vertical effective stress  $\sigma'_{v0}$ , for the soil  
 153 type 1 having plasticity index  $PI = 0$ , are shown in Fig. 1 (b).



154  
 155 (a) (b)  
 156 Fig. 1. Normalized shear modulus reduction curves obtained by Darendeli formulation [33]  
 157 (a) for the four soil types associated to different plasticity index  $PI$  and a given depth  $z = 5 \text{ m}$ ,

158 (b) and for increasing depth  $z$  and a given plasticity index  $PI = 0$ .

159

160 A set of 300 soil profiles is randomly generated with different layer thicknesses and  
161 impedance contrasts, in order to represent various site conditions and estimate the influence of  
162 their uncertainty on the amplification process. Among these 300 soil profiles, for 200 of  
163 them, the shear wave velocity profile increases with depth to consider the effect of increasing  
164 confining stresses. In the other 100 soil profiles, there is an inversion of the shear wave  
165 velocity profile in one of the middle layers. The position and the thickness of the layer with  
166 the shear wave velocity inversion are selected randomly.

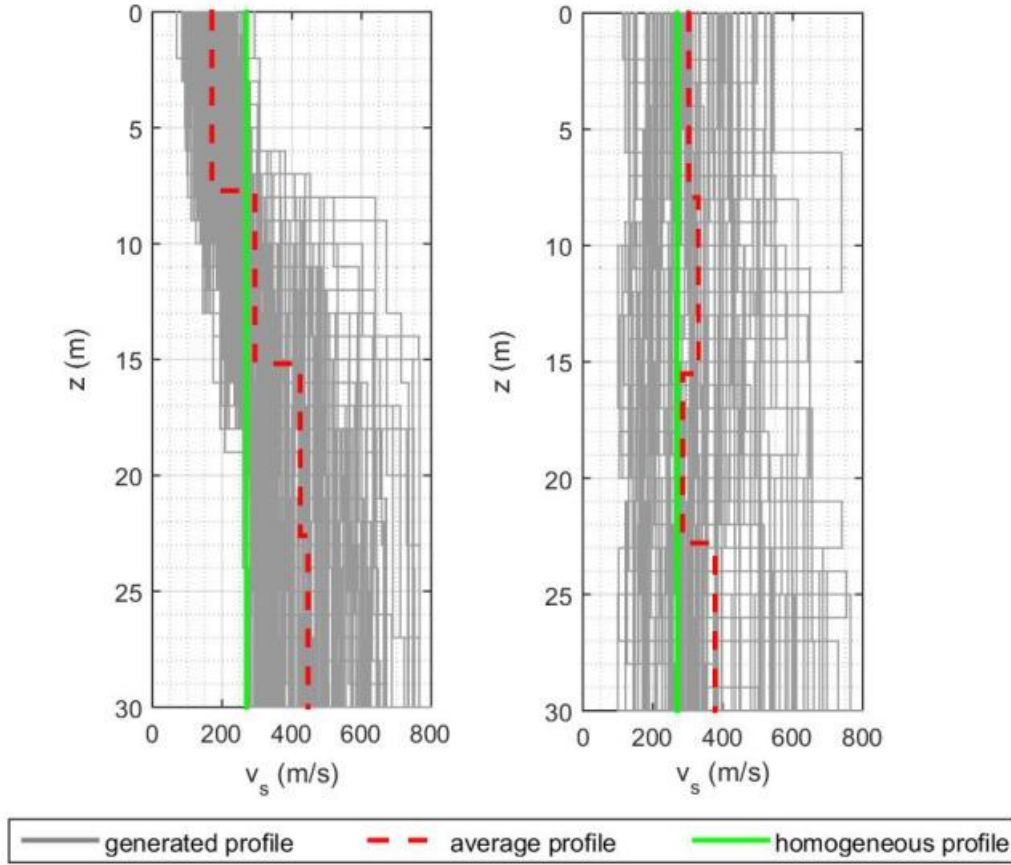
167 The generated shear wave velocity profiles with depth  $v_s(z)$  are shown in Fig. 2, in the cases  
168 of increasing  $v_s$  and of inversions in the profile (a and b, respectively). It can be noted that the  
169 variability in the shear wave velocity profile, according to the same  $v_{s,30} = 270 \text{ m/s}$ , can be  
170 very large.

171

## 172 **2.2 Set of recorded seismic motions**

173 A set of 40 signals, recorded at rock outcrops, is selected as input for the computation of the  
174 seismic wave propagation along the 300 generated soil profiles. These seismic motions  
175 originate from ITACA, the Italian Strong Motion Database [34], ISESD, European Strong  
176 Motion Database [35] or PEER, Pacific Earthquake Engineering Research Center Database  
177 [36].

178 In the adopted set of seismic signals, 20 of them are representative of low to moderate  
179 intensity with magnitudes ranging from 3 to 5.5 (associated to the type 2 response spectrum of  
180 Eurocode 8 [25]) and the other 20 are representative of moderate to high seismicity with  
181 magnitude ranging from 5.6 to 7.5 (type 1 response spectrum).



182

183

184 Fig. 2. Generated shear wave velocity profiles with depth  $v_s(z)$  in the cases of (a) increasing  
 185  $v_s$  and (b) shear wave velocity inversion. All the generated soil profiles have the same  
 186 average shear wave velocity  $v_{s,30} = 270$  m/s .

187

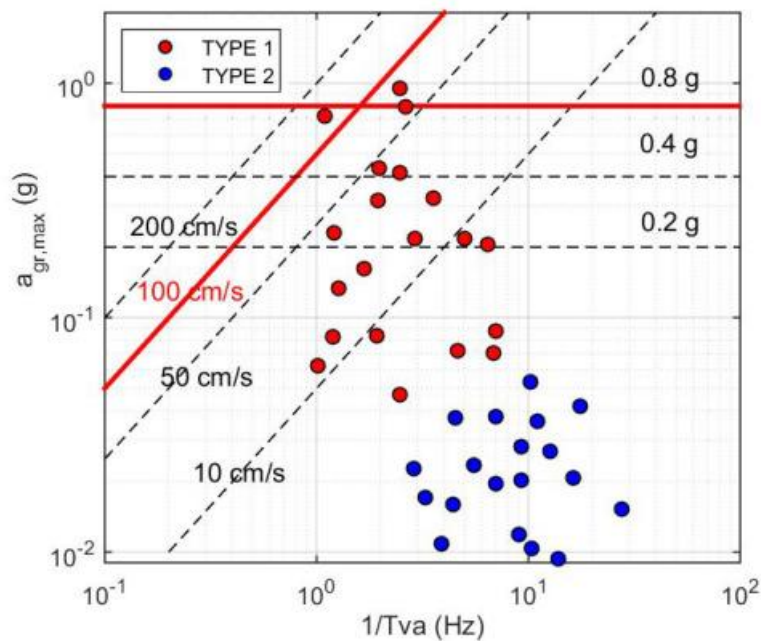
188 Taking into account the influence of the frequency content on the free-field (FF) ground  
 189 motion, the selected seismic records are representative of a wide variety of dominant  
 190 frequencies. The set of recorded seismic motions is sorted in terms of frequency content using  
 191 the equivalent period  $T_{VA}$ , parameter proposed by Cameron and Green [37], defined as

$$192 \quad T_{VA} = 2\pi \frac{\alpha_V(\xi = 5\%) v_{gR}}{\alpha_A(\xi = 5\%) a_{gR}} \quad (2)$$

193 where  $a_{gR}$  and  $v_{gR}$  are the peak ground acceleration and velocity at the outcrop, respectively.

194 The median spectrum amplification factors for horizontal motion are estimated by Newmark  
 195 and Hall [38] as  $\alpha_A(\xi=5\%)=2.12$  and  $\alpha_V(\xi=5\%)=1.65$ , for the constant acceleration and  
 196 constant velocity regions of 5% damped response spectra, respectively.

197 Fig. 3 shows the equivalent predominant frequency  $1/T_{VA}$  related with the peak ground  
 198 acceleration on rock outcrop  $a_{gR}$  for the set of 40 seismic motions. The oblique lines represent  
 199 uniform values of  $v_{gR}$ . The severity of seismic motion increases according to the direction of  
 200 increasing velocity (from the bottom-right corner toward the top-left one, where the values of  
 201  $a_{gR}$  and  $v_{gR}$  are both higher). Based on the observations in Kobe [39], the values  $a_{gR}=0.8g$   
 202 and  $v_{gR}=100\text{cm/s}$  are considered as risk limits, meaning that the input motions above these  
 203 values are considered as the most severe ones (Fig. 3). Then the set of the selected seismic  
 204 motions is made up of a wide variety of frequency content, peak acceleration and peak  
 205 velocity.



206  
 207 Fig. 3. Equivalent predominant frequency  $T_{VA}$  related to the peak ground acceleration at the  
 208 outcrop  $a_{gR}$  for the set of 40 seismic motions. The oblique lines represent uniform values of

209  $v_{gR}$ . The horizontal lines represent constant values of  $a_{gR}$ .

210

### 211 **2.3 Wave propagation model**

212 Assuming a vertical propagation in a horizontally layered medium, the numerical analysis is  
213 undertaken as a one-dimensional approach. The soil is assumed homogeneous and both  
214 assumptions of linear and nonlinear constitutive behavior are analyzed.

215 Quadratic line finite elements are adopted for spatial discretization and the Newmark  
216 algorithm for time discretization, with some numerical damping. The SWAP\_3C finite  
217 element software [30,31,40,41] is used for the numerical simulations.

218 At the soil-bedrock interface, an absorbing boundary condition adopted by Joyner and Chen  
219 [42] is applied in order to take into account the elasticity of the underlying bedrock and allow  
220 energy to be radiated back. The mechanical properties characterizing the bedrock are the  
221 density  $\rho_b$  and the shear wave velocity  $v_{sb}$ .

222 The largest horizontal component of the signal recorded at the reference outcrop is halved and  
223 imposed as the incident wave at the soil-bedrock interface.

224 The finite element size in each soil layer is defined as the minimum between 1m and one  
225 tenth of the minimum wavelength, related to shear wave velocity in the layer and the  
226 maximum frequency assumed equal to 15Hz, above which the spectral content of the input  
227 signal is considered negligible.

228 Details of the finite element model employed in this research are completely described by  
229 Santisi d'Avila et al. [30,31].

230

### 231 **2.4 Hysteretic model for soil**

232 The so-called Masing-Prandtl-Ishlinskii-Iwan (MPII) nonlinear constitutive model [43] is  
233 used for the soil in a total stress analysis. Its main feature is the satisfactory reproduction of

234 nonlinear and hysteretic behavior of soils under cyclic loadings [40,41], starting from the  
235 knowledge of a small number of parameters characterizing the soil properties, such as elastic  
236 parameters and the shear modulus reduction curve.

237 The MPII model is elasto-plastic with linear kinematic hardening. The plasticity model  
238 assumes an associated plastic flow, which allows for isotropic yield. This rheological model  
239 has no viscous damping and the soil damping is purely hysteretic and not frequency  
240 dependent. The size of the Von Mises yield surface is imposed by the backbone curve in the  
241 uniaxial stress case. The tangent constitutive matrix is deduced from the actual strain level  
242 and the strain and stress values at the previous time step [43,44]. [44] This means that the  
243 stress level depends on the strain increment and strain history but not on the strain rate.

244

## 245 **2.5 Data analysis**

246 An optimal selection of site parameters is an important tool for the prediction of the expected  
247 ground motion. Based on recent results [14,22–24], the site dominant frequency  $f_0$  and the  
248 shear wave velocity gradient  $B_{30}$  are chosen as complementary proxies in this study.

249 As proposed by Regnier et al. [45], the shear wave velocity gradient  $B_{30}$  is defined as the  
250 slope of the linear regression of the relation between the logarithm of the shear wave velocity  
251 profile  $v_s(z)$  and the depth  $z$ . Thus, it is computed as:

$$252 \quad \log(v_s(z)) = B_{30} \log(z) + A_{30} \pm \sigma_{30} \quad (3)$$

253 where  $A_{30}$  is the vertical intercept of the regression,  $\sigma_{30}$  is the standard deviation associated to  
254 the linear regression.

255 The shear wave velocity gradient  $B_{30}$ , estimated by Eq. (3) for all the generated 30m deep  
256 soil profiles, quantifies the variation of the shear wave velocity  $v_s(z)$  contrast in the  
257 superficial layers. Its value is close to zero if the velocity is nearly constant with depth and it

258 is larger if the shear wave velocity  $v_s$  increases rapidly with depth [45].

259 The results of the numerical simulations of seismic wave propagation in the set of generated  
260 soil profiles, are first analyzed in terms of amplification factors, according to Ciancimino et  
261 al. [24], in both cases of linear and nonlinear soil behavior.

262 The soil amplification factor  $S_s$  is a local indicator of the site amplification, providing an  
263 estimate of the site effect on the FF motion. It is defined as the ratio of the peak ground  
264 acceleration at the surface  $a_g$  to the peak acceleration at the outcrop  $a_{gR}$  :

$$265 \quad S_s = a_g / a_{gR} \quad (4)$$

266 The spectral amplification factor  $SA$  and the spectral velocity factor  $SV$  are used to quantify  
267 the ground motion intensity in a given period range. These parameters are proposed by Rey et  
268 al. [46]. They are defined as the ratio of  $I_{soil}$  to  $I_{rock}$ . These are the intensity of the spectrum  
269 estimated using the signal at the ground surface and at the outcrop, respectively. The  
270 intensities used in the amplification factors  $SA$  and  $SV$  are calculated by Housner [47] using  
271 the spectrum in terms of acceleration  $PSA(T)$  and velocity  $PSV(T)$ , respectively, as  
272 follows:

$$273 \quad SA = \frac{I_{soil}}{I_{rock}} \quad \text{with} \quad I = \int_{T_1}^{T_2} PSA(T) dT \quad (5)$$

$$274 \quad SV = \frac{I_{soil}}{I_{rock}} \quad \text{with} \quad I = \int_{T_1}^{T_2} PSV(T) dT \quad (6)$$

275 In Eqs (5) and (6),  $[T_1 - T_2]$  is the fixed range of vibration period.

276 In this research, the spectra  $PSA(T)$  and  $PSV(T)$  are normalized with respect to the peak  
277 acceleration at the outcrop  $a_{gR}$ . The period range  $[0.05 - 2.5\text{s}]$ , representative of the  
278 fundamental vibration period for more common structures, is divided into three sub-ranges in  
279 order to analyze the results for short, middle and long periods of vibration. Spectral

280 amplification factors for short [0.05–0.5s], middle [0.5–1s] and long [1–2.5s] periods of  
281 vibration are indicated as  $(SA_S, SV_S)$ ,  $(SA_M, SV_M)$  and  $(SA_L, SV_L)$ , respectively.

282 In a second phase, the response spectra of numerical FF motion are compared to those  
283 suggested by Eurocode 8 [25]. Finally, the results in terms of site amplification factors are  
284 compared with the Eurocode 8 [25], the New Zealand Standard [26] building codes, and those  
285 evaluated by Pitilakis et al. [18], Ciancimino et al. [24].

286

### 287 **3. Results and discussion**

288 The variability of the shear wave velocity profiles with depth  $v_s(z)$  for the set of generated  
289 soil profiles, having the same average  $v_{s,30} = 270$  m/s, is shown in Fig. 2. The FF motion  
290 obtained by numerical simulation, propagating the set of recorded seismic signals along the  
291 generated soil profiles is analyzed.

292 In the following, the influence on site amplification of complementary parameters as the shear  
293 wave velocity profiles with depth  $v_s(z)$ , the site dominant frequency  $f_0$  and the shear wave  
294 velocity gradient  $B_{30}$  is assessed. The fluctuation of amplification factors with the site  
295 parameters  $f_0$  and  $B_{30}$  is analyzed.

296

#### 297 **3.1 Site parameter variability**

298 The dominant frequency of the site  $f_0$  is obtained by evaluating the FF to bedrock transfer  
299 function (TF) that is the ratio of the Fourier spectrum of the accelerograms at the FF soil  
300 surface and at the outcropping bedrock surface. A low-amplitude signal is used so that the soil  
301 remains in the elastic regime. The frequency corresponding to the peak of this TF corresponds  
302 to the fundamental frequency of the soil column, considered as the dominant frequency of the  
303 site  $f_0$ . In the case of a homogeneous soil, the fundamental frequency of a 30m deep soil

304 profile, having a shear wave velocity  $v_s = 270 \text{ m/s}$ , is also deduced [48] as  
305  $f_0 = v_s / (4H) = 2.25 \text{ Hz}$ . The homogeneous soil profile is adopted in the following  
306 comparisons as canonical case.

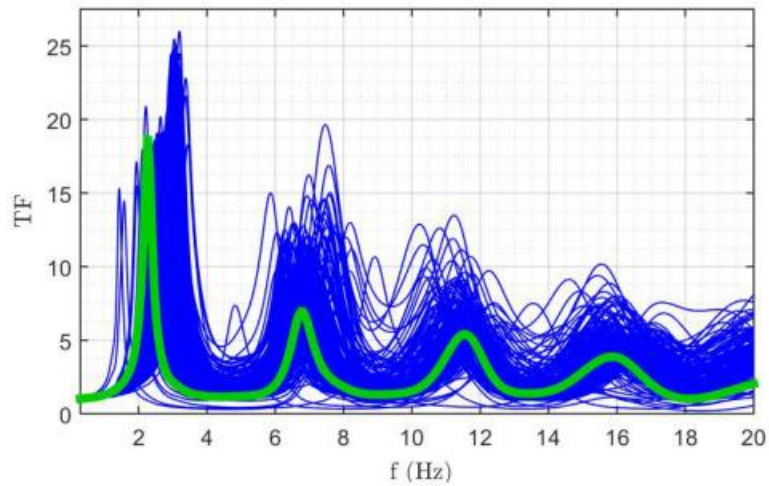
307 Fig. 4 displays the TF obtained for the soil profile with a homogeneous soil, the generated soil  
308 profiles with increasing shear wave velocity with depth  $v_s(z)$  and those with an inversion in  
309 the  $v_s(z)$  profile. The dominant frequency of the site  $f_0$ , obtained for the set of all the  
310 generated soil profiles ranges from 1.5 to 3.5 Hz. For increasing  $v_s(z)$  profiles (Fig. 4a), the  
311 dominant frequency of the site is mostly higher than the frequency for the homogeneous case.  
312 Whereas the natural frequencies obtained for soil profiles with an inversion in  $v_s(z)$  are  
313 distributed in a frequency range (Fig. 4b). The peaks of the TF obtained for the generated soil  
314 profiles show a higher amplification compared with the homogeneous soil profile in most  
315 cases. In particular, the amplification estimated for the soil profiles having increasing  $v_s(z)$  is  
316 larger for higher  $f_0$  (Fig. 4a).

317 According to Fig. 4, the site amplification changes depending on the stratigraphy (i.e. shear  
318 wave profile with depth  $v_s(z)$ ) and the fundamental frequency of the site  $f_0$ . The frequency  
319 content of the surface motion varies accordingly.

320 Fig. 5 illustrates the linear correlation between the shear wave velocity gradient  $B_{30}$  and the  
321 fundamental frequency of the site  $f_0$ , for the set of generated soil profiles with given  $v_{s,30}$ .  
322 This correlation is high, with a correlation coefficient  $r^2 = 0.85$ , for the whole set of 300 soil  
323 profiles.

324 The amplification factors in Eqs (4), (5) and (6) are calculated using the computed FF motion  
325 and the related response spectrum for all the 24000 samples (set of 40 recorded seismic  
326 signals applied to 300 generated soil profiles, for linear and nonlinear soil behaviors).

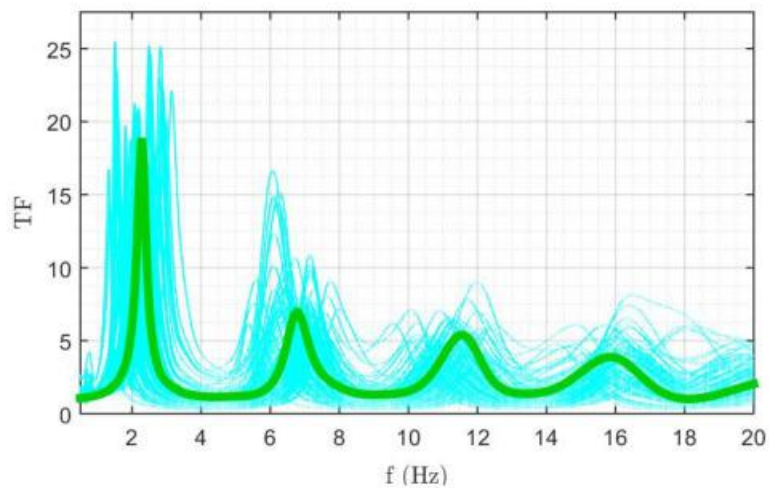
327 The estimated amplification factors  $S_s$ ,  $SA$  and  $SV$ ,  $SA_s$ ,  $SA_M$  and  $SA_L$ ,  $SV_s$ ,  $SV_M$  and  $SV_L$ ,  
328 are shown in Figs 6, 7, 8, and 9 as functions of the dominant period of the site  $T_0 = 1/f_0$  and  
329 of the shear wave velocity gradient  $B_{30}$ , respectively, for both cases of linear (a) and nonlinear  
330 (b) behavior. The trend of mean and standard deviation is also displayed by the thick and  
331 dashed lines, respectively.



332

333

(a)



334

335

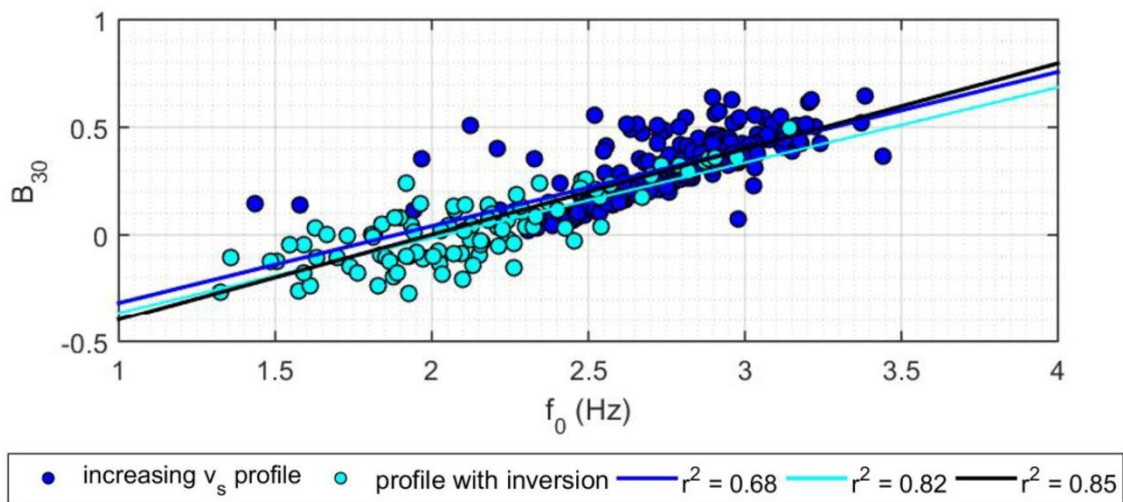
(b)

336 Fig. 4. Free-field to bedrock transfer function for the generated deep soil profiles having  
337 increasing shear wave velocity profile (a) and showing a velocity inversion (b). The thick line  
338 is the transfer function for the homogeneous soil profile.

339

340 Figs 6, 7, 8 and 9 illustrate the amplification factors in the three fixed ranges of period in  
341 order to understand if their variation is modified for different periods. It appears that the  
342 largest amplifications are reached for short vibration periods (lower than 0.5 s).

343 Figs 6 and 8 display that site amplification is strongly dependent on the site predominant  
344 period  $T_0$ , for short vibration periods of the FF motion ( $SA_S, SV_S$ ) and independent from it for  
345 long periods ( $SA_L, SV_L$ ). Moreover, site amplification is much more pronounced in soil  
346 profiles having  $T_0$  lower than that of the homogeneous profile, for short vibration periods of  
347 the FF motion ( $SA_S, SV_S$ ). Whereas, for middle periods of vibrations ( $SA_M, SV_M$ ), site  
348 amplification is more pronounced in soil profiles having predominant period  $T_0$  higher than  
349 that of the homogeneous profile.

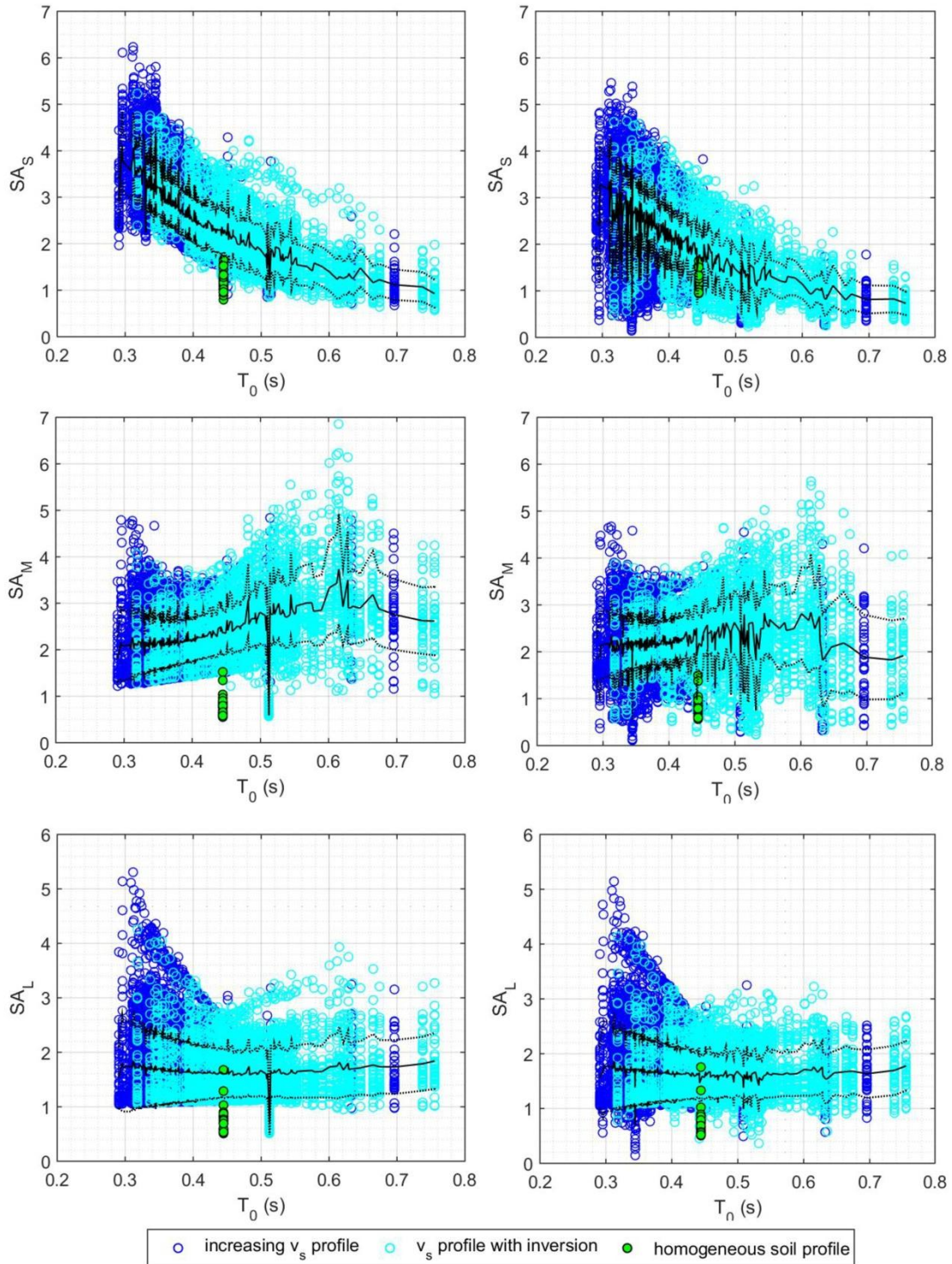


351 Fig. 5. Linear regression of the shear wave velocity gradient  $B_{30}$  with reference to the  
352 fundamental frequency of the site  $f_0$ , for the generated deep soil profiles. The thick line is for  
353 the set of all 300 generated soil profiles.

354

355 Figs 7 and 9 show that the largest values of amplification factors are reached for short

356 vibration periods of the FF motion ( $SA_S, SV_S$ ), lower than 0.5 s, in soil profiles having a high  
 357 shear wave velocity gradient  $B_{30}$ , which corresponds to sites with a large impedance contrast  
 358 in the first 30 m or with a steep slope in shear wave velocity profile.



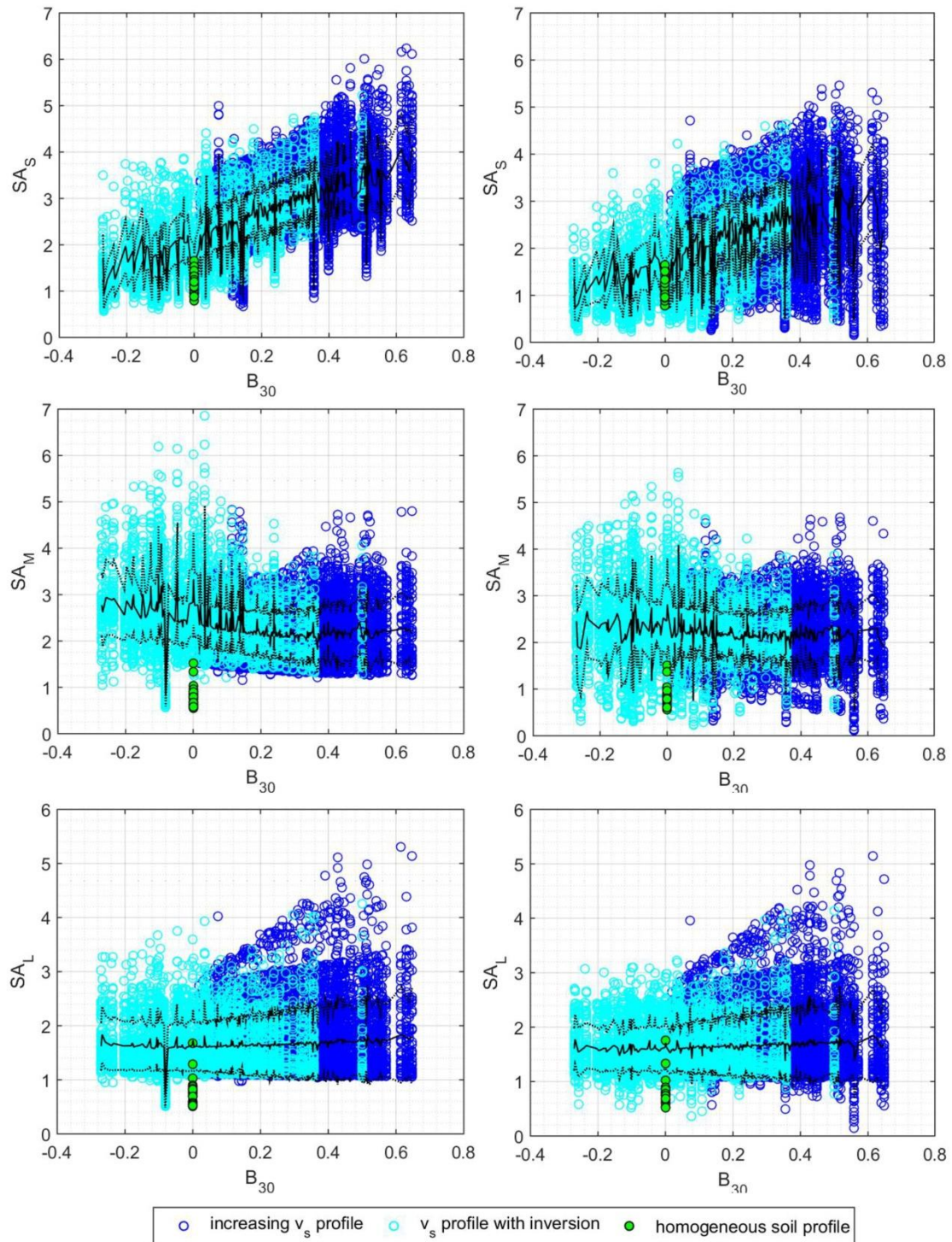
359

360

(a)

(b)

361 Fig. 6. Amplification factors  $SA_S$ ,  $SA_M$  and  $SA_L$  as a function of the dominant period of the  
 362 site  $T_0$ , for both cases of linear (a) and nonlinear (b) behaviors. The thick and dashed lines  
 363 represent the mean and means plus one standard deviation (SD) trend.



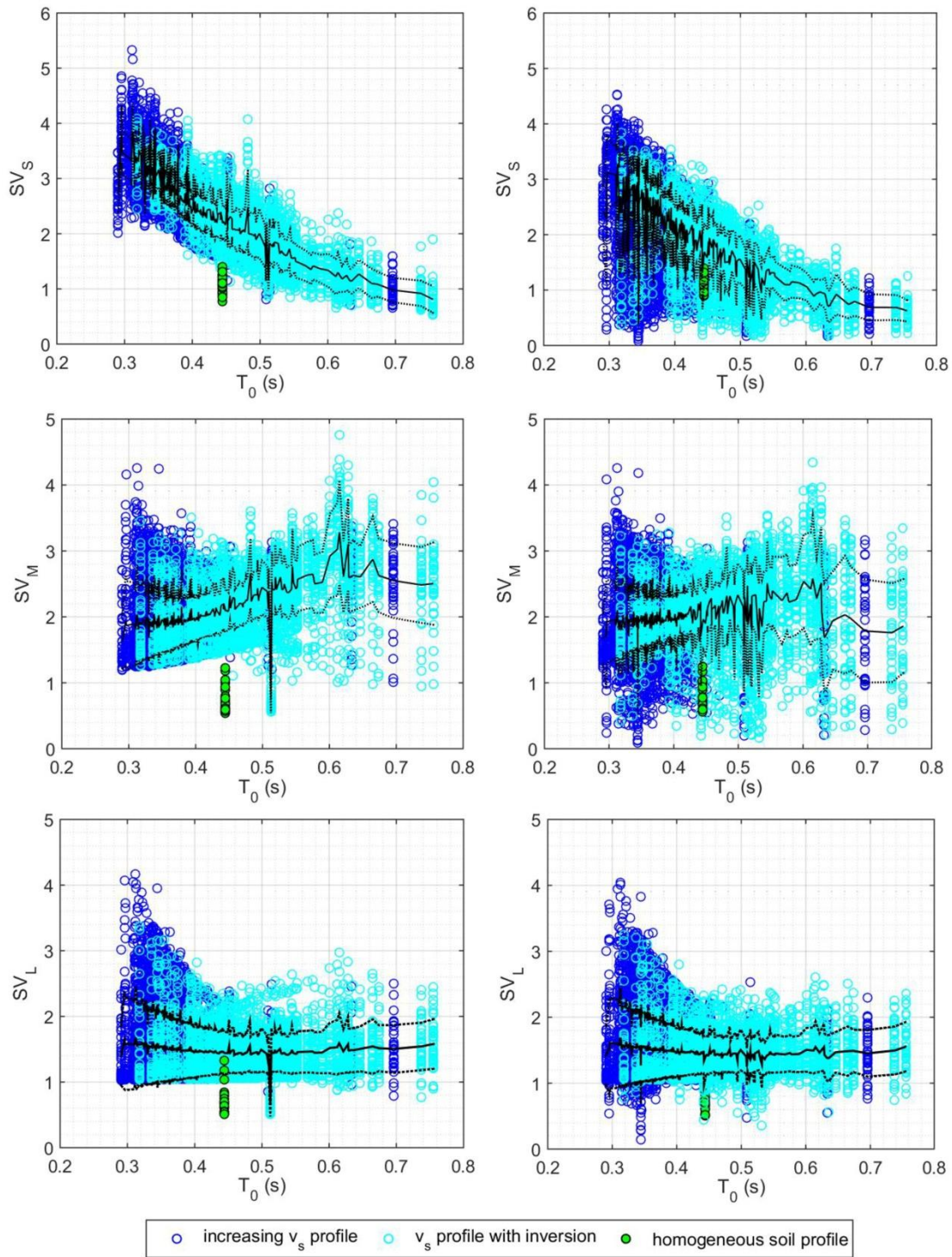
364

365

(a)

(b)

366 Fig. 7. Amplification factors  $SA_S$ ,  $SA_M$  and  $SA_L$  as a function of the shear wave velocity  
 367 gradient  $B_{30}$ , for both cases of linear (a) and nonlinear (b) behaviors. The thick and dashed  
 368 lines represent the mean and means plus one standard deviation (SD) trend.



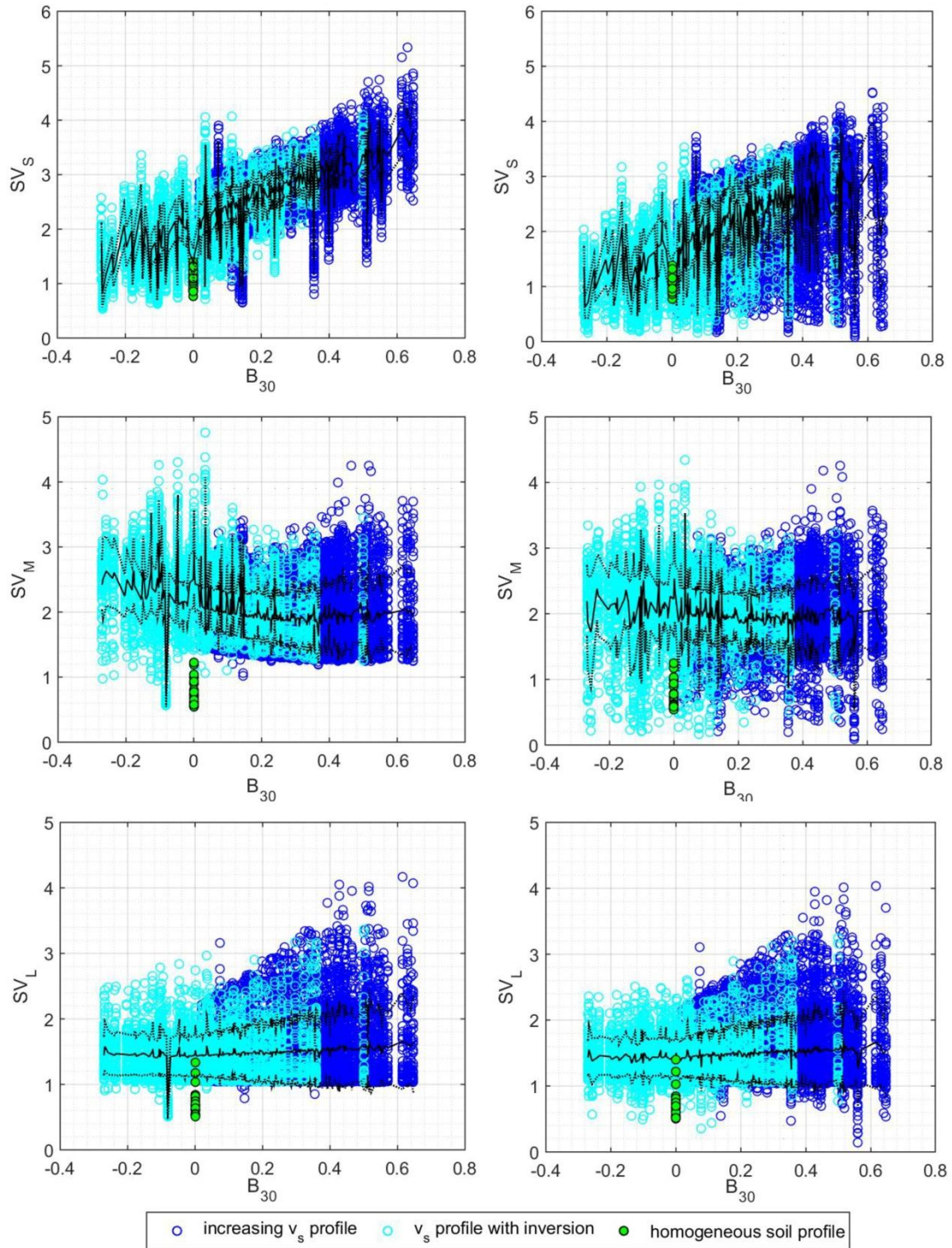
369

370

(a)

(b)

371 Fig. 8. Amplification factors  $SV_S$ ,  $SV_M$  and  $SV_L$  as a function of the dominant period of the  
 372 site  $T_0$ , for both cases of linear (a) and nonlinear (b) behaviors. The thick and dashed lines  
 373 represent the mean and means plus one standard deviation (SD) trend.



374

375

(a)

(b)

376 Fig. 9. Amplification factors  $SV_S$ ,  $SV_M$  and  $SV_L$  as a function of the shear wave velocity  
377 gradient  $B_{30}$ , for both cases of linear (a) and nonlinear (b) behaviors. The thick and dashed  
378 lines represent the mean and means plus one standard deviation (SD) trend.  
379 The nonlinear soil behavior on the site response induces a reduced amplification effect.  
380 Similarly to the case of linear soil behavior, the site amplification is more pronounced in the  
381 case of short vibration periods of the FF motion and it is strongly dependent on the proposed  
382 site parameters. On the contrary, the site amplification is less pronounced and independent  
383 from the proposed site parameters, for longer vibration periods of the FF motion.

384

### 385 **3.2 Influence on site effects of the nonlinear soil behavior**

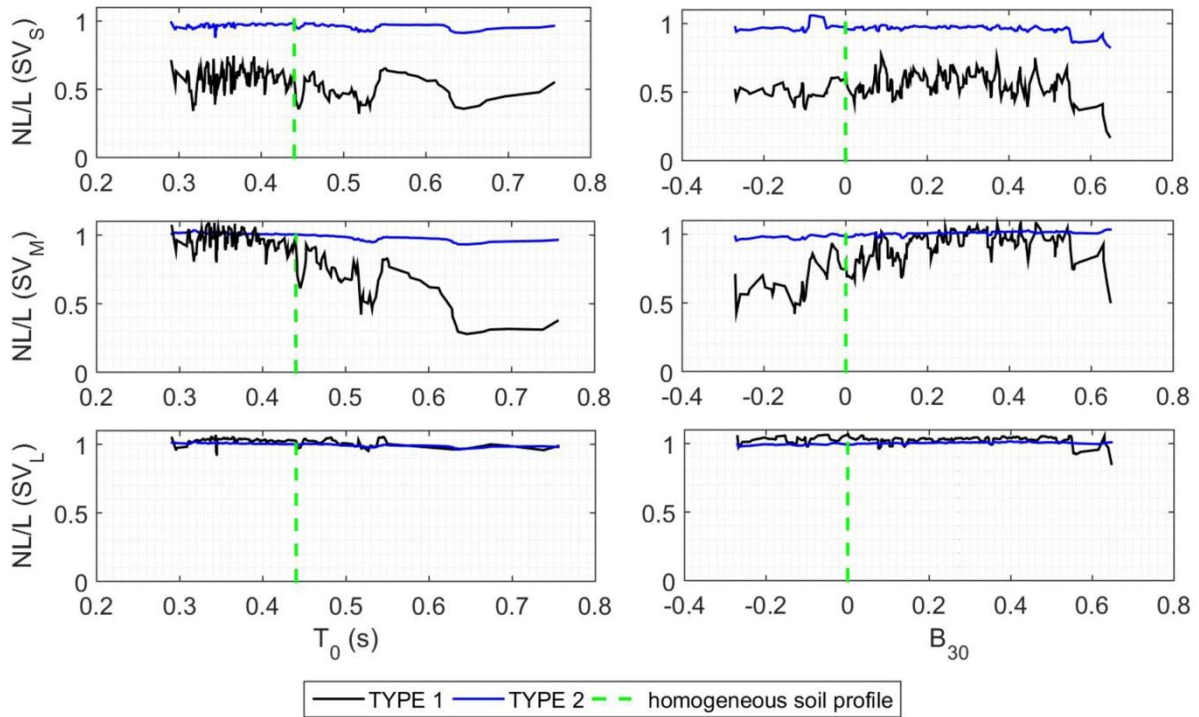
386 In this section, the effects of soil nonlinearities on site response are investigated with  
387 reference to the proposed site proxies (predominant period  $T_0$  and shear wave velocity  
388 gradient  $B_{30}$ ). The main goal is to verify the reliability of  $T_0$  and  $B_{30}$  even in the range of soil  
389 nonlinear behavior. The impact of nonlinear soil response on the site response is characterized  
390 in terms of amplification factor  $SV$ . The  $SV$  factor is estimated in both cases of linear and  
391 nonlinear soil response, in the three adopted period ranges. The amplification factor  $NL/L$  is  
392 computed as the ratio of spectral velocity factors  $SV_S$ ,  $SV_M$  and  $SV_L$  in the ranges of short,  
393 middle and long period, for nonlinear soil behavior to that for linear soil behavior.

394 Fig.10 illustrates the average amplification factor as a function of the site dominant period  $T_0$   
395 (Fig. 10a) and shear wave velocity gradient  $B_{30}$  (Fig. 10b). Results are distinguished between  
396 those for weak earthquakes (associated to the type 2 response spectrum of Eurocode 8 [25])  
397 and strong earthquakes (type 1 response spectrum).

398 As expected, the effect of nonlinear soil behavior is negligible for small earthquakes (type 2  
399 response spectrum of Eurocode 8 [25]) for the whole range of periods of vibration. In fact, the

400  $NL/L$  ratio is close to one.

401 In the case of stronger earthquakes (type 1 response spectrum), the modification in the site  
402 response depends on the stratigraphy and varies with the vibration period of the FF motion.



403

(a)

(b)

404

405 Fig. 10. Computed ratio of spectral velocity factors  $SV_S$ ,  $SV_M$  and  $SV_L$  (short, intermediate  
406 and long periods of vibration) for nonlinear soil behavior to that for linear soil behavior  
407 ( $NL/L$ ) as a function of the dominant period of the site  $T_0$  (a) and the shear wave velocity  
408 gradient  $B_{30}$  (b), for the whole set of generated soil profiles. The curves are distinguished  
409 between those for small earthquakes (associated to the type 2 response spectrum of Eurocode  
410 8) and strong earthquakes (type 1 response spectrum).

411

412 According to Fig. 10, for vibration periods of the strong motion over 1s, the effect of  
413 nonlinear soil behavior is negligible (see  $SV_L$ ). On the contrary, in the range of short periods  
414 (see  $SV_S$ ), the amplitude reduction due to nonlinear effects is up to 60%. Moreover, the

415 amplification factor in the range of middle periods (see  $SV_M$ ) show a remarkable amplitude  
416 reduction for a site predominant period  $T_0$  higher than 0.44s (period of vibration of the  
417 homogeneous soil profile) and a reduction up to 10% for lower periods  $T_0$  (Fig 10a). An  
418 important amplitude reduction is obtained for a shear wave velocity gradient  $B_{30}$  outside the  
419 range  $[0-0.5]$ , that correspond to soil profiles with significant impedance contrast (high  $B_{30}$ )  
420 and velocity inversions (negative  $B_{30}$ ).

421

### 422 **3.4 Comparison with building codes**

423 Fig. 11 displays the comparison of the average pseudo-acceleration response spectrum  
424 normalized with respect to the peak acceleration of the outcropping motion, using a damping  
425 ratio of 5% .

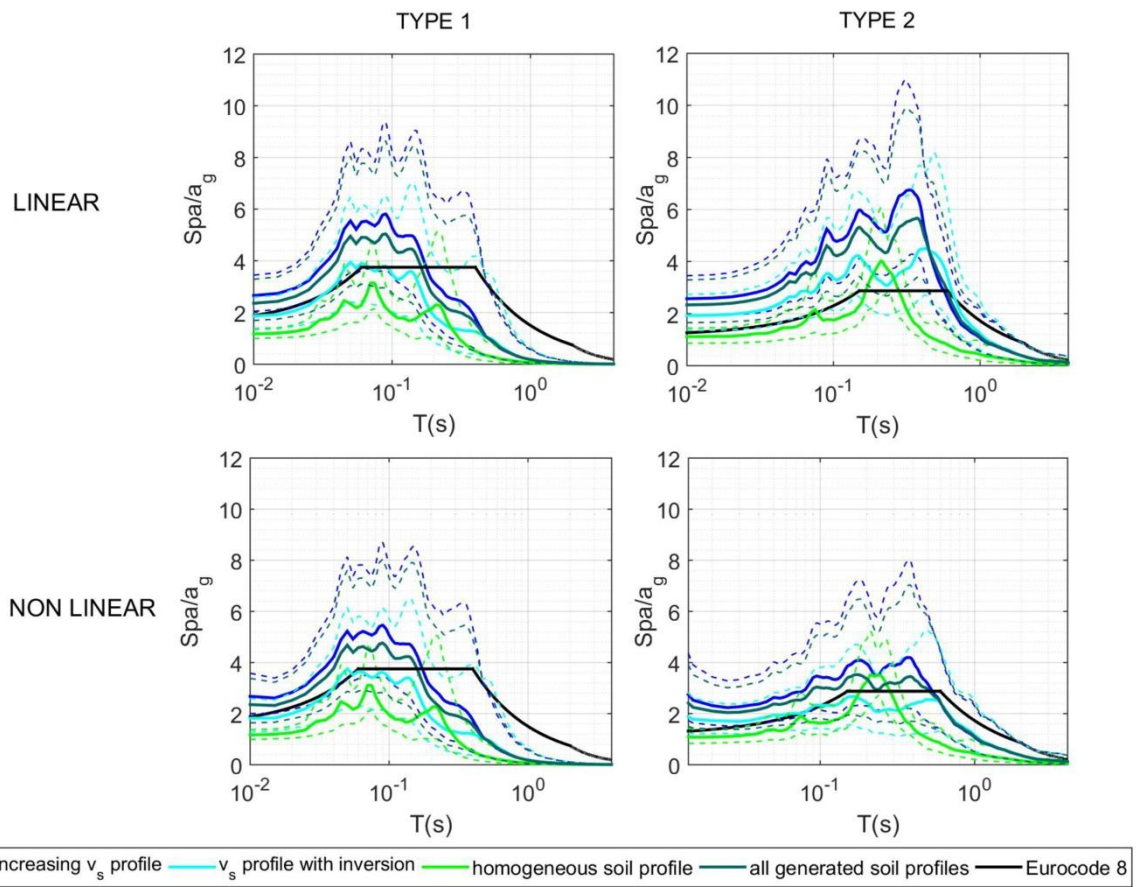
426 The linear and nonlinear computations are separated and, for both, the cases of weak  
427 earthquakes (associated to the type 2 response spectrum of the Eurocode 8 [25]) and strong  
428 earthquakes (type 1 response spectrum) are distinguished. In each of these combinations, the  
429 average pseudo-acceleration response spectra are estimated for the FF motion in the case of  
430 increasing shear wave velocity and for profiles with a velocity inversion.

431 The elastic response spectra proposed by Eurocode 8 is conservative, compared to the  
432 obtained average response spectra, for higher periods (higher than 0.2s for type 2 and 0.6s  
433 for type 1). Conversely, for lower periods, the average response spectrum, obtained for all the  
434 generated soil profiles, gives higher acceleration peaks.

435 If the elastic response spectrum proposed by Eurocode 8 [3] is compared for the spectrum in  
436 the homogeneous case, with average soil properties, it is conservative for the whole ranges of  
437 period for weak earthquakes (type 2) and in most cases for strong earthquakes (type 1).

438 The reduction of the site response for the nonlinear soil behavior is negligible for weak

439 earthquakes (type 2) and significant for strong earthquakes (type 1).



440

441

442

443

444

445

446

447

448

449

450

451

452

(a) (b)

Fig. 11. Mean (solid line) acceleration response spectra (damping ratio of 5% ) and mean plus one standard deviation (dashed line), evaluated for the free-field motion of the generated multilayered soil profiles, compared to the homogeneous case and the elastic response spectrum proposed by Eurocode 8 [3]. The cases are distinguished as follows: assumption of linear and nonlinear soil behavior; weak earthquakes (a) and strong earthquakes (b). Following the approach adopted by Ciancimino et al. [24] for the linear regime, the site amplification factors are evaluated for the samples of the present statistical analysis, in the case of linear and nonlinear soil behavior. The computed amplification factors are compared with those suggested by Eurocode 8 [25] and New Zealand Standard [26] building codes, with those proposed by Pitilakis et al. [18] and with those obtained by Ciancimino et al. [24]. The ground type classification used in the Eurocode 8 [25] is only based on the  $v_{s,30}$  parameter. In

453 the New Zealand Standard [26], the fundamental site period is included as a proxy of site  
454 effects. In addition, Pitilakis et al. [18] classify the ground type using the fundamental period  
455 of the site, the depth of the seismic bedrock and the average soil column shear wave velocity  
456 are taken into account. The 300 generated soil profiles are identified as ground type C  
457 according to Eurocode 8 [25] and as C2 according Pitilakis et al. [18]. Among them, 286 are  
458 identified as ground type C according to the New Zealand Standard [26] building codes  
459 ( $T_0 > 0.6s$ ).

460 The comparison between the mean value of site amplification factors  $S_s$  (Eq. (4)) and  $SA$   
461 (Eq. (5)), and the values within one standard deviation of the mean are represented in Fig. 12  
462 for weak earthquakes and in Fig. 13 for strong earthquakes. These values are compared to  
463 those obtained according to the building codes to analyze their reliability. The coefficient of  
464 variation  $CV$  of  $S_s$  and  $SA$  is also calculated. In each figure, the simulations under the  
465 assumption of linear and nonlinear soil behavior are separated. The amplification factors are  
466 estimated, for both soil behaviors, using only the FF motions of multilayered soil profiles with  
467 increasing shear wave velocity with depth, only the FF motions of soil profiles with a velocity  
468 inversion, the FF motions of all the generated soil profiles and the FF motion of the  
469 homogeneous soil profile.

470 The obtained numerical results obtained under the assumption of linear soil behavior are also  
471 compared to those obtained by Ciancimino et al. [24], that performed analyses on a database  
472 of seismic responses of one-dimensional soil profiles having equivalent linear behavior. We  
473 can observe that our results under the assumption of linear behavior are in good agreement  
474 with those obtained by Ciancimino et al. [24].

475 According to Figs 12 and 13, only the amplification factors obtained for the case of  
476 homogeneous soil profile are smaller than those suggested by Eurocode 8 [25] and the same  
477 consideration is made comparing with the New Zealand Standard [26] building codes (Fig.

478 14).

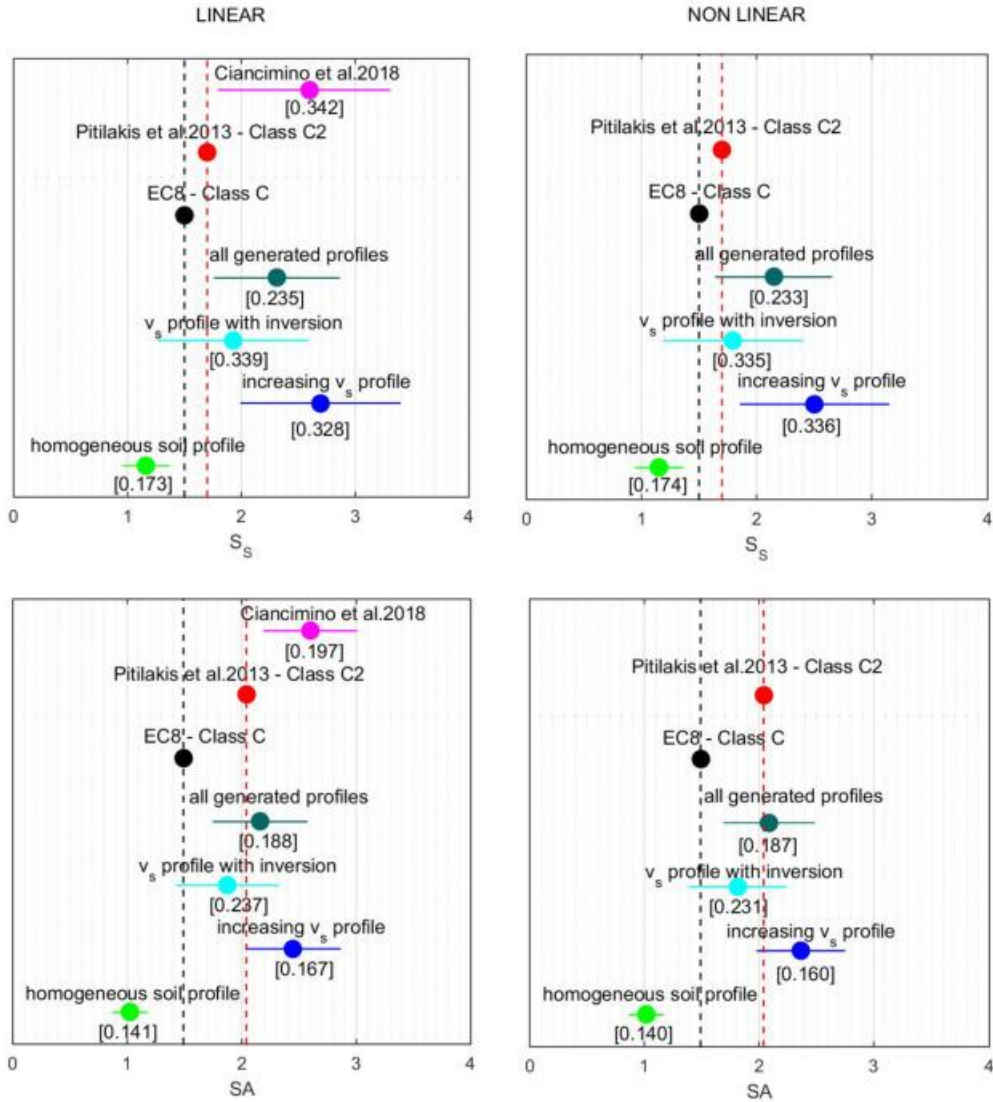
479 It is interesting to note that the values proposed by Pitilakis et al. [18] for the site  
480 amplification factor  $SA$  are close to those computed using the set of generated samples in the  
481 present analysis. Conversely, the values proposed by Pitilakis et al. [18] for the site  
482 amplification factor  $S_s$  are lower than those obtained in the present research. This means that  
483 ground classification based on complementary site proxies instead on a single proxy is more  
484 adequate. But also it is important to understand the best complementary proxies that allow  
485 predicting the site response for different ranges of periods.

486 Moreover, the nonlinear effects are negligible in terms of mean values and  $CV$  of the  
487 amplification factors, for weak earthquakes (Fig. 12) and they are significant for strong  
488 earthquakes (Fig. 13).

489 The average amplification factors obtained for soil profiles with a velocity inversion are lower  
490 than the ones associated to other soil profiles.

491 Lastly, Fig. 14 shows that the comparison between the computed amplification factors and  
492 those deduced by New Zealand Standard [26]. The difference observed could be justified by a  
493 higher seismicity expected in New Zealand that could increase the effect of nonlinear soil  
494 behavior and thus reduce the peak acceleration.

TYPE 2



495

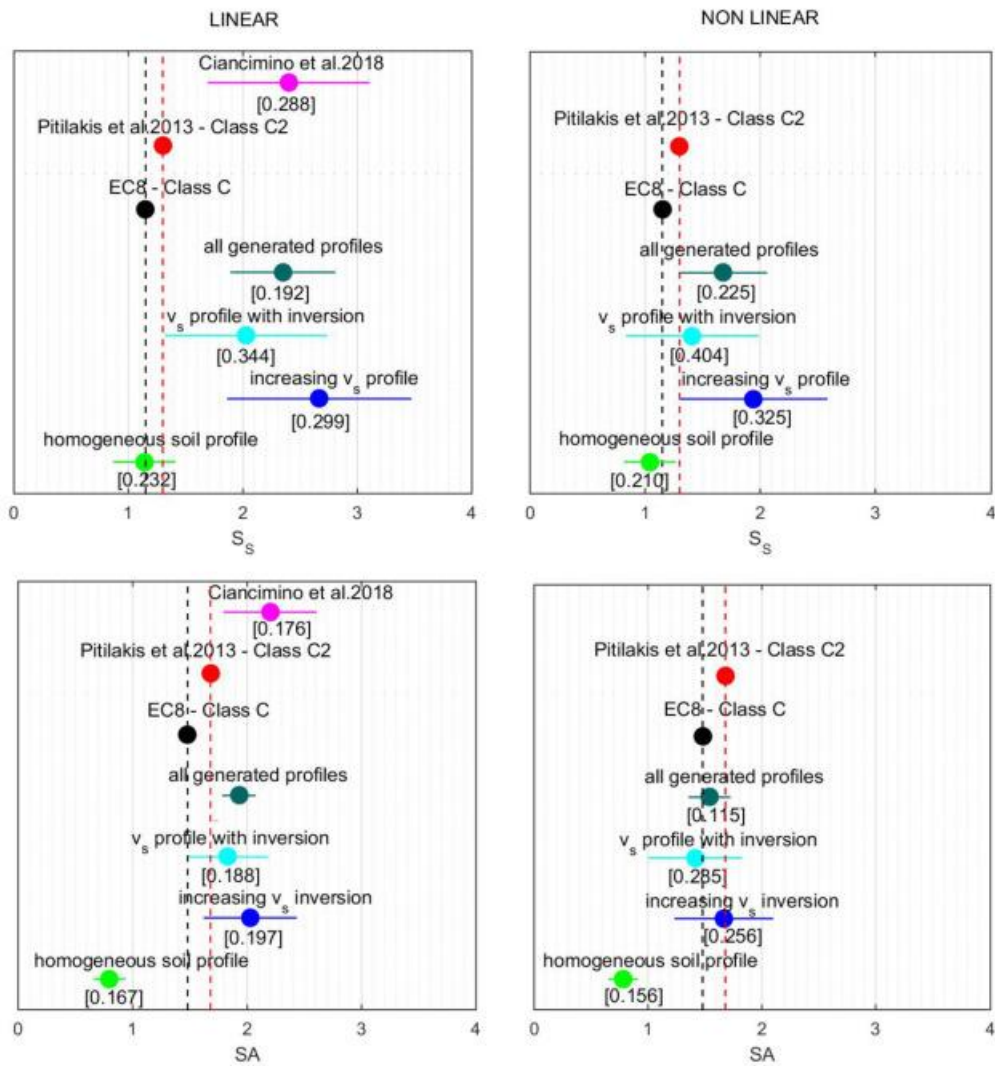
496

(a)

(b)

497 Fig. 12. Mean value of site amplification factors  $S_s$  (top) and  $SA$  (bottom), the values within  
 498 one standard deviation of the mean and the coefficient of variation  $CV$  (value between  
 499 brackets) in the case of small earthquakes (type 2 response spectrum of Eurocode 8 [25]), for  
 500 numerical simulations under the assumption of linear (a) and nonlinear (b) soil behavior. The  
 501 values suggested by Eurocode 8 [25], Pitilakis et al. [18] and Ciancimino et al [24] are  
 502 indicated.

TYPE 1



(a)

(b)

503

504

505 Fig. 13. Mean value of site amplification factors  $S_s$  (top) and  $SA$  (bottom), the values within

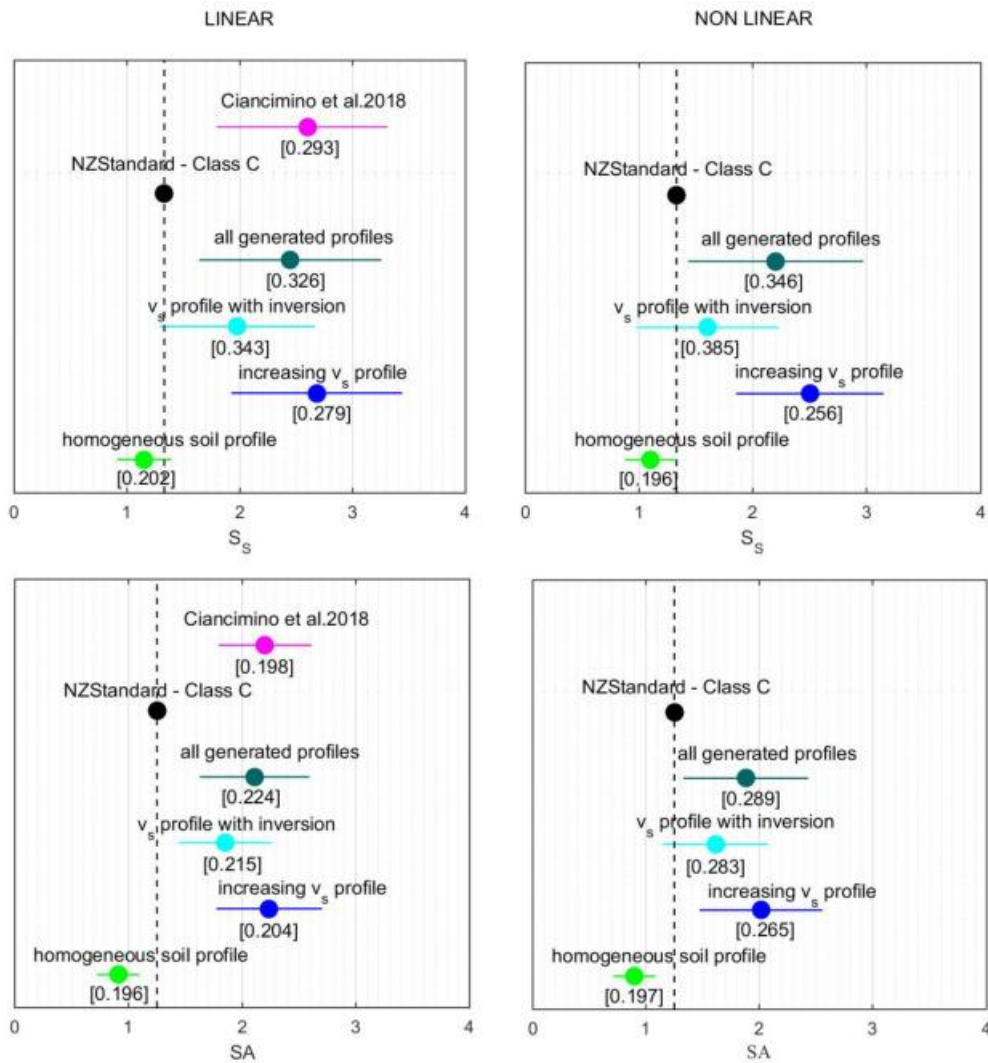
506 one standard deviation of the mean and the coefficient of variation  $CV$  (value between

507 brackets) in the case of strong earthquakes (type 1 response spectrum of Eurocode 8 [25]), for

508 numerical simulations under the assumption of linear (a) and nonlinear (b) soil behavior. The

509 values suggested by Eurocode 8 [25], Pitilakis et al. [18] and Ciancimino et al [24] are

510 indicated.



511

512

(a)

(b)

513 Fig. 14. Mean value of site amplification factors  $S_s$  (top) and  $SA$  (bottom), the values within

514 one standard deviation of the mean and the coefficient of variation  $CV$  (value between

515 brackets) for the whole set of recorded seismic signals. Numerical simulations under the

516 assumption of linear (a) and nonlinear (b) soil behavior are separated. The values suggested

517 by the New Zealand Standard [26] building codes are indicated.

518

#### 519 4. Conclusions

520 The vertical propagation of various recorded seismic signals along stochastically generated

521 soil profiles is numerically simulated to obtain the FF motion, in both cases of linear and

522 nonlinear soil behavior. The average shear wave velocity in the upper 30m of soil profiles  
523  $v_{s,30}$  is fixed and corresponds to the ground type C, according to the Eurocode 8. The soil-  
524 bedrock interface depth is selected as  $H_{800} = 30$  m .

525 This research highlights the influence of the layering uncertainty on the site response. It is  
526 demonstrated that the average shear wave velocity  $v_{s,30}$  is not able, as single parameter, to  
527 characterize the soil profiles in terms of expected amplification level over the whole  
528 frequency range.

529 Two site parameters are proposed as proxies, complementary to  $v_{s,30}$ , such as the dominant  
530 frequency of the site  $f_0$  and the shear wave velocity gradient  $B_{30}$  . The site response is  
531 represented in terms of site amplification factors, deduced using the response spectrum of the  
532 FF motion, for the 24000 performed simulations (set of 40 recorded seismic signals applied to  
533 300 generated soil profiles, for linear and nonlinear soil behaviors). The influence on site  
534 amplification of the shear wave velocity profile, site dominant frequency and shear wave  
535 velocity gradient are analyzed independently from  $H_{800}$  .

536 The obtained amplification factors are functions of both site conditions and intensity of rock  
537 motions and the values could decrease due to soil nonlinearity. The amplification factors  
538 increase with decreasing site dominant period  $T_0$  and increasing shear wave velocity gradient  
539  $B_{30}$  , when they are evaluated over a large range of vibration periods  $[0.05-2.5s]$  .

540 Nevertheless, site amplification appears strongly dependent on the site predominant period  
541  $T_0$ , for short vibration periods of the FF motion and independent from it for long periods.  
542 Moreover, site amplification is much more pronounced in soil profiles having  $T_0$  lower than  
543 that of the homogeneous profile, for short vibration periods of the FF motion.

544 The largest values of amplification factors are reached for short vibration periods of the FF  
545 motion, lower than 0.5s , in soil profiles having a high shear wave velocity gradient  $B_{30}$  ,

546 which corresponds to sites with a large impedance contrast in the first 30m or with a steep  
547 slope in the shear wave velocity profile.

548 The site response is modified when the nonlinear soil behavior is taken into account in the  
549 numerical simulations. The nonlinear soil behavior on the site response induces a reduced  
550 amplification effect. Similarly to the case of linear soil behavior, the site amplification is more  
551 pronounced in the case of short vibration periods of the FF motion and it is strongly  
552 dependent on the proposed site parameters. On the contrary, the site amplification is less  
553 pronounced and independent from the proposed site parameters, for vibration periods of the  
554 FF motion higher than 1s.

555 Nonlinear effects are negligible for small earthquakes and for vibration periods of strong  
556 ground motions longer than 1s. Whereas, they are significant for short- and middle-periods of  
557 strong earthquakes. In particular, soil profiles having dominant period  $T_0$  higher than that of  
558 the homogeneous profile exhibit significant nonlinear effects. In addition, soil profiles with  
559 negative value of  $B_{30}$  (i.e. velocity inversion) and profiles with high value of  $B_{30}$  lead to  
560 pronounced nonlinear site effects.

561 Average amplification factors are compared to those suggested by Eurocode 8 [25] and New  
562 Zealand Standard [26] building codes, and by Pitilakis et al. [18]. The obtained results  
563 demonstrate that the ground type classification proposed by Eurocode 8 [25], based on  $v_{s,30}$   
564 only, is not suitable. The comparison to the amplification factors proposed by Pitilakis et al.  
565 [18] shows that the introduction of complementary site proxies makes the ground type  
566 classification more adequate. In fact, the computed average spectral amplification factors  $SA$   
567 are comparable to those estimated by Pitilakis et al. [18].

568 The average amplification factors computed for soil profiles with a velocity inversion are  
569 lower than for the profiles having monotonic shear wave velocity profiles.

570 This research confirms that it is possible to improve the current ground type classification

571 taking into account simple and accessible site parameters complementary to  $v_{s,30}$ . Accounting  
572 for complementary site proxies in the ground type classification, such as the dominant  
573 frequency of the site  $f_0$  and the shear wave velocity gradient  $B_{30}$ , allow a better prediction of  
574 the expected amplification, in particular for short vibration periods of the FF motion, up to 1 s.  
575 Further work should be done to analyze the results for soil profiles having different ground  
576 types according to the Eurocode 8 (only ground type C has been discussed in this research)  
577 and depth  $H_{800}$ .

578

## 579 **6. References**

- 580 [1] Semblat JF, Kham A, Parara E, Bard P, Pitilakis K, Makra K, et al. Seismic wave  
581 amplification : Basin geometry vs soil layering . Soil Dynamics and Earthquake Eng.  
582 2005; 25(7-10):529-538. 2009.
- 583 [2] Borchardt RD. Estimates of site-dependent response spectra for design (methodology  
584 and justification). Earthq Spectra 1994;10:617–53.
- 585 [3] Dickenson, S. E. and RBS. Nonlinear dynamic response of soft and deep cohesive soil  
586 deposits. Proc. Int. Work. site response Subj. to strong Earthq. motions, 1996, p. 67–  
587 81.
- 588 [4] Dobry, R., Borchardt, R. D., Crouse, C. B., Idriss, I. M., Joyner, W. B., Martin, G. R.,  
589 Seed RB. New site coefficients and site classification system used in recent building  
590 seismic code provisions. Earthq Spectra 2000;16:41–67.
- 591 [5] Seyhan, E., Stewart, J. P., Ancheta, T. D., Darragh, R. B., & Graves RW. NGA-West2  
592 site database. Earthq Spectra 2014;30:1007–24. doi:10.1193/062913EQS180M.
- 593 [6] Seyhan E, Stewart JP. Semi-Empirical Nonlinear Site Amplification from NGA-West2  
594 Data and Simulations. Earthq Spectra 2014;30:1241–56.  
595 doi:10.1193/063013EQS181M.

- 596 [7] Derras B, Bard PY, Cotton F. Site-condition proxies, ground motion variability, and  
597 data-driven GMPEs: Insights from the NGA-West2 and RESORCE data sets. *Earthq*  
598 *Spectra* 2016;32:2027–56. doi:10.1193/060215EQS082M.
- 599 [8] Park D, Hashash YMA. Probabilistic seismic hazard analysis with non linear site  
600 effects in the Mississippi embayment. 13 th World Conf. *Earthq. Eng.*, 2004, p. 1549.
- 601 [9] Mucciarelli M, Gallipoli MR. Comparison between Vs30 and other estimates of site  
602 amplification in Italy. *First Eur Conf Earthq Eng Seismol* 2006:270.
- 603 [10] Castellaro S, Mulargia F, Rossi PL. Vs30: Proxy for Seismic Amplification? *Seismol*  
604 *Res Lett* 2008;79:540–3. doi:10.1785/gssrl.79.4.540.
- 605 [11] Cadet H, Bard PY, Duval AM. a New Proposal for Site Classification Based on  
606 Ambient Vibration Measurements and the Kiknet Strong Motion Data Set. 14th World  
607 Conf *Earthq Eng* 2008.
- 608 [12] Luzi L, Puglia R, Pacor F, Gallipoli MR, Bindi D, Mucciarelli M. Proposal for a soil  
609 classification based on parameters alternative or complementary to Vs,30. *Bull Earthq*  
610 *Eng* 2011;9:1877–98. doi:10.1007/s10518-011-9274-2.
- 611 [13] Cadet H, Bard PY, Duval AM, Bertrand E. Site effect assessment using KiK-net data:  
612 Part 2-site amplification prediction equation based on f0 and Vsz. *Bull Earthq Eng*  
613 2012;10:451–89. doi:10.1007/s10518-011-9298-7.
- 614 [14] Derras B, Bard PY, Cotton F. VS30, slope, H800 and f0: Performance of various site-  
615 condition proxies in reducing ground-motion aleatory variability and predicting  
616 nonlinear site response 4. *Seismology. Earth, Planets Sp* 2017;69:0–21.  
617 doi:10.1186/s40623-017-0718-z.
- 618 [15] Castelli F, Cavallaro A, Grasso S, Lentini V. Seismic microzoning from synthetic  
619 ground motion earthquake scenarios parameters: The case study of the city of Catania  
620 (Italy). *Soil Dyn Earthq Eng* 2016;88:307–27. doi:10.1016/j.soildyn.2016.07.010.

- 621 [16] Steidl JH. Site response in southern California for probabilistic seismic hazard analysis.  
622 Bull Seismol Soc Am 2000;90:149–69. doi:10.1785/0120000504.
- 623 [17] Kotha, S. R., Cotton, F., & Bindi D. A New Approach to Site Classification : Mixed-  
624 effects Ground Motion Prediction Equation with Spectral Clustering of Site  
625 Amplification Functions. Soil Dyn Earthq Eng 2018;110:318–29.
- 626 [18] Pitilakis K, Riga E, Anastasiadis A. New code site classification, amplification factors  
627 and normalized response spectra based on a worldwide ground-motion database. Bull  
628 Earthq Eng 2013;11:925–66. doi:10.1007/s10518-013-9429-4.
- 629 [19] Castellaro S, Mulargia F. Simplified seismic soil classification: The Vfz matrix. Bull  
630 Earthq Eng 2014;12:735–54. doi:10.1007/s10518-013-9543-3.
- 631 [20] Zhao JX, Irikura K, Zhang J, Fukushima Y, Somerville PG, Asano A, et al. An  
632 empirical site-classification method for strong-motion stations in Japan using H/V  
633 response spectral ratio. Bull Seismol Soc Am 2006;96:914–25.  
634 doi:10.1785/0120050124.
- 635 [21] Gallipoli MR, Mucciarelli M. Comparison of site classification from VS30, VS10, and  
636 HVSR in Italy. Bull Seismol Soc Am 2009;99:340–51. doi:10.1785/0120080083.
- 637 [22] Boudghene Stambouli A, Zendagui D, Bard PY, Derras B. Deriving amplification  
638 factors from simple site parameters using generalized regression neural networks:  
639 Implications for relevant site proxies. Earth, Planets Sp 2017;69. doi:10.1186/s40623-  
640 017-0686-3.
- 641 [23] Zhu C, Pilz M, Cotton F. Which is a better proxy, site period or depth to bedrock, in  
642 modelling linear site response in addition to the average shear-wave velocity? Bull  
643 Earthq Eng 2019:1–24. doi:10.1007/s10518-019-00738-6.
- 644 [24] Ciancimino A, Foti S, Lanzo G. Stochastic analysis of seismic ground response for site  
645 classification methods verification. Soil Dyn Earthq Eng 2018;111:169–83.

- 646 doi:10.1016/j.soildyn.2018.04.006.
- 647 [25] European Committee for Standardization (CEN). Eurocode 8: Design of structures for  
648 earthquake resistance—Part 1: General rules, seismic actions and rules for buildings  
649 (EN 1998-1: 2004). Eur Comm Norm Brussels 2004.
- 650 [26] 1170.5:2004 NZS. Structural Design Actions - Part 5: Earthquake actions- New  
651 Zealand. Struct Des Actions 2004.
- 652 [27] Brûlé S, Javelaud E. H/V method in geotechnical engineering. Application to a two  
653 layers model. Rev Fr Geotech 2013;142.
- 654 [28] Régnier J, Cadet H, Bonilla LF, Bertrand E, Semblat JF. Assessing Nonlinear Behavior  
655 of Soils in Seismic Site Response : Statistical Analysis on KiK-net Strong-Motion  
656 Data. Bull Seismol Soc Am 2013;103:1750–70. doi:10.1785/0120120240.
- 657 [29] Régnier J, Cadet H, Bard PY. Empirical quantification of the impact of nonlinear soil  
658 behavior on site response. Bull Seismol Soc Am 2016;106:1710–9.  
659 doi:10.1785/0120150199.
- 660 [30] Santisi d’Avila MP, Lenti L, Semblat JF. Modelling strong seismic ground motion:  
661 Three-dimensional loading path versus wavefield polarization. Geophys J Int  
662 2012;190:1607–24. doi:10.1111/j.1365-246X.2012.05599.x.
- 663 [31] Santisi d’Avila MP, Semblat JF, Lenti L. Strong ground motion in the 2011 Tohoku  
664 earthquake: A one-directional three-component modeling. Bull Seismol Soc Am  
665 2013;103:1394–410. doi:10.1785/0120120208.
- 666 [32] Yokota K, Imai T, Konno M. Dynamic deformation characteristics of soils 1981:13–  
667 37.
- 668 [33] Darendeli MB. Development of a new family of normalized modulus reduction and  
669 material damping curves. PhD thesis, The University of Texas at Austin, 2001.
- 670 [34] Massa M, Pacor F, Luzi L, Bindi D, Milana G, Sabetta F, et al. The Italian

- 671 ACcelerometric Archive (ITACA): Processing of strong-motion data. *Bull Earthq Eng*  
672 2010. doi:10.1007/s10518-009-9152-3.
- 673 [35] Ambraseys NN, Smit P, Douglas J, Margaris B, Sigbjörnsson R, Ólafsson S, et al.  
674 Internet site for European strong-motion data. *Boll Di Geofis Teor Ed Appl*  
675 2004;45:113–29.
- 676 [36] PEER PEERC. PEER Ground Motion Database. *Shallow Crustal Earthquakes Act*  
677 *Tecton Regimes, NGA-West2 2013.*
- 678 [37] Cameron WI, Green RA. Soil Nonlinearity versus Frequency Effects. *Int Work*  
679 *Uncertainties Nonlinear Soil Prop Their Impact Model Dyn Response 2004:1–7.*
- 680 [38] Newmark NM, Hall WJ. *Earthquake Spectra and Design, Earthquake Engineering*  
681 *Research Center. Berkeley, CA 1982:103.*
- 682 [39] Kawase H. Strong motion characteristics and their damage impact to structures during  
683 the off pacific coast of tohoku earthquake of march 11, 2011: How extraordinary was  
684 this M 9. 0 earthquake. *4th IASPEI/IAEE Int. Symp., 2011.*
- 685 [40] Régnier J, Bonilla LF, Bard PY, Bertrand E, Hollender F, Kawase H, et al.  
686 International benchmark on numerical simulations for 1D, nonlinear site response  
687 (Prenolin): Verification phase based on canonical cases. *Bull Seismol Soc Am*  
688 2016;106:2112–35. doi:10.1785/0120150284.
- 689 [41] Régnier J, Bonilla LF, Bard PY, Bertrand E, Hollender F, Kawase H, et al. Prenolin:  
690 International benchmark on 1D nonlinear: Site-response analysis—validation phase  
691 exercise. *Bull Seismol Soc Am* 2018;108. doi:10.1785/0120170210.
- 692 [42] Joyner WB, Chen ATF. Calculation of nonlinear ground response in earthquakes. *Bull*  
693 *Seismol Soc Am* 1975;65:1315–36.
- 694 [43] Iwan W.D. On a class of models for the yielding behavior of continuous and composite  
695 systems. *J Appl Mech* 1967;34:612–7.

- 696 [44] Joyner WB. A method for calculating nonlinear seismic response in two dimensions.  
697 Bull Seismol Soc Am 1975;65:1337–57.
- 698 [45] Régnier J, Bonilla LF, Bertrand E, Semblat JF. Influence of the VS profiles beyond 30  
699 m depth on linear site effects: Assessment from the KiK-net Data. Bull Seismol Soc  
700 Am 2014;104:2337–48. doi:10.1785/0120140018.
- 701 [46] Rey J, Faccioli E, Bommer JJ. Derivation of design soil coefficients (S) and response  
702 spectral shapes for Eurocode 8 using the European Strong-Motion Database. J Seismol  
703 2002;6:547–55. doi:10.1023/A:1021169715992.
- 704 [47] Housner GW. Spectrum Intensities of Strong-Motion Earthquakes. Symp Earthq Blast  
705 Eff Struct 1952:20–36.
- 706 [48] Kramer S. Geotechnical Earthquake Engineering. Prentice H. Upper Saddle River:  
707 1996.
- 708